Facies analysis of yedoma thermokarst lakes on the northern Seward Peninsula, Alaska

Louise Farquharson [a,*], Katey Walter Anthony [b], Nancy Bigelow [c], Mary Edwards [c, d], Guido Grosse [e]

[a]Department of Geoscience, Reichardt Building, 900 Yukon Drive, University of Alaska Fairbanks, Fairbanks, AK, 99775, USA

[b]Water and Environmental Research Center, University of Alaska Fairbanks, Fairbanks, AK, 99775, USA

[c]Alaska Quaternary Center, University of Alaska Fairbanks, Fairbanks, AK, 99775, USA

[d]Geography and Environment, University of Southampton, Highfield, Southampton SO17 1BJ, UK

[e]Alfred Wegener Institute Helmholtz Centre for Polar and Marine Research, 14473 Potsdam, Germany

Corresponding author.

E-mail address: lmfarquharson@alaska.edu (L.Farquharson)

Phone: (+1) 907 451 7184

Abstract

Thermokarst lakes develop as a result of the thaw and collapse of ice-rich, permanently frozen ground (permafrost). Of particular sedimentological importance are thermokarst lakes forming in late Pleistocene icy silt (yedoma), which dramatically alter the land surface by lowering surface elevation and redistributing upland sediment into lower basins. Our study provides the first description of yedoma thermokarst lake sedimentology based on cross-basin sampling of an existing lake. We present lake-sediment facies descriptions based on data from sediment cores from two thermokarst lakes of medium depth, Claudi and Jaeger (informal names), which formed in previously non thermokarst-affected upland yedoma on the northern Seward Peninsula, Alaska. We identify four prominent facies using sedimentological, biogeochemical and macrofossil indicators: a massive silt lacking aquatic macrofossils and other aquatic indicators situated below a sub-lacustrine unconformity (Facies 1); two basal deposits: interbedded organic silt and chaotic silt (Facies 2 - 3); and a silt-rich mud (Facies 4). Facies 1 is interpreted as yedoma that has thawed during lake formation. Facies 3 formed adjacent to the margin due to thaw and collapse events from the lake shore. Material from Facies 3 was reworked by wave action to form Facies 2 in a medium energy margin environment. Facies 4 formed in a lower energy environment towards the lake basin center. This facies classification and description should enhance our ability to i) interpret the spatial and temporal development of lakes, and ii) reconstruct long-term patterns of landscape change.

Key words: Permafrost, yedoma, thermokarst lake, sedimentology, facies

1. Introduction

Thermokarst landforms are prevalent across arctic and sub-arctic lowlands (Jorgenson et al., 2008a, 2008b) and include features such as thermokarst lakes and drained lake basins (Grosse et al., 2013, and references therein), thermo-erosion gullies (Godin and Fortier, 2012), retrogressive thaw slumps (Burn and Lewkowicz, 1990) and thermokarst pits (Osterkamp et al., 2000; Jorgenson et al., 2006). Thermokarst lakes and drained lake basins are the most ubiquitous of these landforms (Côté and Burn, 2002; Hinkel et al., 2005; Jones et al., 2011; Morgenstern et al., 2011), contributing to landscape evolution by redistributing large volumes of sediment (Murton, 1996) and initiating changes in surface elevation, topography, vegetation composition (Katamura et al., 2006), wildlife habitat (Jorgenson and Osterkamp, 2005), and hydrology (Yoshikawa, 2003). In areas of yedoma (silty, organic rich, perennially frozen sediment containing massive syngenetic Pleistocene ice wedges; Schirrmeister et al., 2013), thermokarst lakes and drained lake basins are abundant, affecting up to 73% of the land surface (Jones et al., 2011; Grosse et al., 2013) (Fig. 1). Herein we refer to yedoma soils as 'organic rich' in the context of mineral soils (as opposed to peat).

Thermokarst lakes forming in yedoma uniquely develop from the gradual thaw of large syngenetic Pleistocene ice-wedge networks. Thermokarst lakes usually initiate due to a disturbance to the ground thermal regime (e.g., wildfire or climate warming; Burn and Smith, 1990; Murton, 2009) which results in the thaw of excess ground ice, collapse of the ground surface, and subsequent collection of water in a closed depression (Van Everdingen, 1988; French, 1996). Thermokarst lakes go through distinct stages of development that likely cause shifts in sediment composition as well as both vertical and lateral sediment distribution (Czudek and Demek, 1970; Murton, 1996; West and Plug, 2008). After initial ponding, water body diameter and depth continue to increase via lateral thermo-erosion and vertical thaw settlement, respectively, forming a lake (Burn, 1992). In our study area on the northern Seward Peninsula, Alaska, the upland margins that characterize first-generation lakes (those forming in upland yedoma as opposed to drained lake basin lowlands) today expand at mean rates of 0.18 m/yr, while regional rates including all margin types are 0.39 m/yr (Jones et al., 2011). Settlement depths (the height difference between surrounding bluff tops and the bottom of the lake water column) of up to 40 m have been reported for yedoma deposits in central Yakutia (Czudek and Demek, 1970). Remnant mounds of sediment, termed baydjerakhs, remain once massive syngenetic ice wedges have thawed (Kanevskiy et al., 2011). These mounds are an important characteristic of yedoma thermokarst lake bathymetry, especially along lake margins. As lake development continues and the water depth becomes greater than maximum winter lake ice thickness, ice-rich yedoma deposits beneath the lake thaw year round (Ling et al., 2012). This area of continuously thawed sediment beneath a water body is termed a “thaw bulb” or "talik" (West and Plug, 2008), and the sediments within it are termed “taberal” (Hubberten and Romanovskii, 2003). Taberal sediments are therefore originally deposited subaerially but thawed and modified in situ underneath the lake.

Numerous papers have investigated morphological aspects of thermokarst lake behaviour, such as lake orientation (Livingstone, 1954; Côté and Burn, 2002), lake cycling (Billings and Peterson, 1980; Jorgenson and Shur, 2007), lake drainage (Mackay, 1988; Hinkel et al., 2003; Marsh et al., 2009), lake influence on arctic landscape evolution (Czudek and Demek, 1970; Soloviev, 1973), and development of thermokarst sedimentology and morphology (Burn and Smith, 1990; Murton, 1996; Morgenstern et al., 2013). Yet currently there is a knowledge gap regarding the sedimentology and geomorphological development of modern day yedoma thermokarst lakes.

Our goal was to better understand yedoma thermokarst lake development by studying sediment cores from two first-generation lakes that formed in upland yedoma on the northern Seward Peninsula, Alaska. Specific objectives were to establish 1) the key facies present, 2) the depositional environment represented by each facies, and 3) the stages of lake development based on vertical and horizontal facies distribution. Sediment composition, the range of depositional facies present and facies distribution are used to infer relative stages of lake development. We chose to study first-generation thermokarst lakes as they would have been most prevalent across yedoma lowlands during the early Holocene, a time during which such lakes likely contributed significantly to high-latitude atmospheric methane flux (Walter et al., 2007a; Brosius et al., 2012; Walter Anthony et al., 2014). Results from this study should improve our ability to date thermokarst lake development more accurately and aid the reconstruction of landscape evolution during the late Pleistocene and Holocene. Furthermore, they may allow for a better understanding of their past and present role in carbon cycling in the Arctic and aid modeling of thermokarst landscape evolution.

2. Study area

We studied the composition and distribution of sediment in Claudi Lake in detail, and supplemented this data set with additional cores from Jaeger Lake (Figs. 1, 2, Table 1). Claudi Lake is a first-generation lake that formed in upland yedoma. Claudi Lake is oval in shape, has a lake surface area of 16.27 ha and a maximum depth of 9.2 m. A paleo-drainage channel has eroded the north bank of the lake and appears close to reactivation. The southern margin of Claudi Lake is eroding into a first-generation drained lake basin, that of former Pear Lake (Plug and West, 2009).

Jaeger Lake is a first generation lake that also formed in yedoma upland. An active outlet is located on the western margin. Jaeger Lake is hourglass in shape, has a lake surface area of 24.06 ha and a maximum depth of 12.73 m. The bathymetry of lakes Claudi and Jaeger is characterized by the presence of baydjerakhs. The variable microtopography they create affects local sediment distribution in the lake bed (Hopkins and Kidd, 1988). The macrophyte zones of both Claudi and Jaeger are sparsely vegetated by *Hippuris* spp., *Carex aquatillis* and *Calamagrostis canadensis*.

The study area is located in the coastal lowlands of the northern Seward Peninsula, Alaska, on the eastern side of the Bering Strait (Fig. 1). This region has abundant thermokarst lakes and several large maar lakes (Arp and Jones, 2009). Surficial geology is dominated by late Pleistocene ice-rich syngenetic yedoma deposits and Holocene lacustrine and bog deposits (Hopkins and Kidd, 1988; Charron, 1995; Jones et al., 2012; Wetterich et al., 2012). Widespread thermokarst development in the Arctic is thought to have last occurred during the Holocene thermal maximum (Walter et al., 2007a; Mann et al., 2010), suggesting that this was the time period when many lakes in our study area, now drained lake basins, developed. Remote sensing-based morphological and succession studies of drained lake basins suggest that up to 6 generations of Holocene lake basins are overlapping in the study region, indicating a landscape actively shaped by thermokarst lake dynamics (Jones et al., 2012; Regmi et al., 2012). One single lake generation represents a cycle of thaw and collapse, lake formation, lake drainage, epigenetic ice aggradation, and the eventual initiation of a new thermokarst lake in the same location. Within this study, we refer to areas that have not yet been affected by thermokarst processes as “upland” while areas that have been affected by thermokarst lake processes are termed “lowland” (Fig. 2).

The Yedoma deposits consist mostly of organic-rich, silty to fine-sandy sediments with interspersed paleosols (Höfle and Ping, 1996; Höfle et al., 2000; Kuzmina et al., 2008). Networks of syngenetic ice-wedge polygons are widely distributed across upland areas, while landscape degradation has created widespread accumulation of lacustrine and taberal sediments, often modified by epigenetic ice wedge formation. Extensive basaltic tephra deposits from the eruption of Devil Mountain Maar lake ca. 18 ^{14}C kyr BP (Beget et al., 1996; Goetcheus and Birks, 2001) can be greater than 1 m thick at the study sites and lie 0.6-3.0 m below the modern day surface in undisturbed upland yedoma deposits (Charron, 1995; Goetcheus and Birks, 2001).

Present day vegetation is moist acidic shrub tundra dominated by *Salix* (willow), *Betula* (birch), and heaths or *Eriophorum* (cotton grass) tussocks. Upland vegetation is characterized by low shrubs: *Empetrum nigrum* (crowberry), *Vaccinium uliginosum* (blueberry), *Betula nana* and *B. glandulosa*. Steep upland yedoma slopes adjacent to lake margins are dominated by *Salix* spp., *B. nana*, *Spiraea stevenii*, *Ledum palustre* (labrador tea) and grasses. Floodplains and drained lake basins are moister and dominated by taxa such as *Eriophorum* spp., *Carex aquatillis* (water sedge), *Sphagnum riparium* (streamside sphagnum) and *Calamagrostis canadensis* (reed grass).

Climate is maritime in summer due to proximity to the ice-free Bering Sea, and continental in winter. The mean annual air temperature is -4.8°C, with a mean summer temperature of 10.5°C (June through August) and a mean winter temperature of -13.7°C (October through April). The mean annual precipitation is 273 mm for the period July 1996 to December 2008 (Western Regional Climate Center, Western U.S. Climate Historical Summaries, http://www.wrcc.dri.edu, 01/15/15).

3. Methods

3.1 Fieldwork

We retrieved sediment cores during two field campaigns on the northern Seward Peninsula. In Spring 2009, we retrieved 44 cores (Claudi Lake, n=33, Jaeger Lake, n=11) using ice that was more than 1 m thick as a platform from 23 coring locations across both lakes (Fig. 1, not all coring locations shown). Core length retrieved in 2009 totaled 30 m. In Summer 2010, we obtained an additional 20 cores from Claudi Lake using a floating coring platform from 7 coring locations (Fig. 1, not all coring locations shown). Core length retrieved in 2010 totaled 10 m. The length of all 64 cores combined totaled 40 m. Mean core length was 60 cm, ranging from 10 cm to 110 cm. At Claudi Lake, N-S and E-W bathymetric transects were recorded across the entire lake at 100 m spacing, providing an overview of the lake’s bathymetry (see Fig. 2 in Kessler et al., 2012). At each coring site, a more detailed N-S and an E-W 1 x 1 m grid of bathymetric measurements was collected across a 10 x 10 m area (see Fig. 7 in Walter Anthony and Anthony, 2013). This enabled us to determine the location of coring sites with respect to baydjarakh mounds. We used different coring systems depending on water depths and targeted core lengths. Upper sediments were obtained using a square-rod Livingstone corer (Wright et al., 1984) modified to fit a 7 cm polycarbonate barrel (Bolivia corer). We obtained deeper, stiffer, and more compacted sediment using a standard square-rod Livingston corer with a 5 cm metal barrel. Continuous cores containing upper and lower sediment were also obtained with a percussion corer (Reasoner, 1993). We obtained two long, deep cores from the central part of Claudi Lake using a UWITEC© piston corer (8 kg weight and transparent PVC core liners 6.35 cm in diameter). Coring took place until core refusal occurred due to the presence of stiff silt, coarse tephra or peat.

3.2 Laboratory work

We conducted high-resolution sedimentological analysis of lake cores on the sediment-core transects across the study lakes and established facies distributions. On all cores we measured magnetic susceptibility at 1 cm increments downcore using a GEOTEK multi-sensor core logger. We removed anomalously low magnetic susceptibility measurements at core breaks from the data set. We photographed all split cores using a digital line scanner at a resolution of 10 pixels per millimeter (~300 dpi). We described split cores according to Schnurrenberger et al. (2003) and visually identified key facies according to color, composition, texture, boundary type and sedimentary structure. Working with wet sediment we described sediment color using a Munsell color chart.

We analyzed a 9.58 m subset of key cores from Claudi and Jaeger (Claudi, n=11, Jaeger, n=3) for $\delta^{13}C$, percent total organic carbon (TOC), percent total nitrogen (TN), grain size, and macrofossils. For this we selected the deepest cores and also chose a range of cores to ensure a wide geographic spread of samples. For isotope and C and N determinations, we pretreated 100 bulk sediment samples to remove inorganic carbon by overnight acidification using 2N HCl (Claudi, n=83, Jaeger, n= 17; for core locations see Figs. 3 and 4 respectively). Samples were then rinsed with high purity water until neutral (Wolfe et al., 2001), freeze dried, homogenized, weighed (to the nearest 0.001 mg), and submitted to the Alaska Stable Isotope Facility at the University of Alaska Fairbanks's Water and Environmental Research Center. Determinations of $\delta^{13}C$, TOC and % TN were made on a Delta V isotope ratio mass spectrometer interfaced with a Costech ESC 4010 elemental analyzer. Stable isotope ratios are reported for 97 samples in δ notation as parts per thousand (‰) deviation from the international standard for carbon (Pee Dee Belemnite). Typically, analytical precision for elemental and isotopic analysis is <0.2 ‰.

Forty-two grain-size samples from Claudi (for core locations see Fig. 3) were pretreated with hydrogen peroxide (H_2O_2) to remove organics, sodium hydroxide (NaOH) to remove biogenic silica (BSi) and hydrochloric acid (HCl) to neutralize the sodium and remove carbonates. Pretreated samples were then run on a Horiba particle size analyzer LA-920 according to the LacCore (National Lacustrine Core Facility) standard operating procedure based on Jiilavenkatesa et al. (2001) and Horiba particle size analyzer LA-920 manuals.

We processed 68 macrofossil samples using the methods of Birks (2002) (Claudi, n=55, Jaeger, n = 13, for core locations see Figs. 3 and 4 respectively). Wet sample volume was measured using water displacement, samples were then sieved through a 250 µm mesh. Macrofossils were identified using the Alaska Quaternary Center's macrofossil collection at the University of Alaska Fairbanks and reference texts (Katz et al., 1965; Ireland, 1982). Macrofossil counts were standardized to a volume of seven cubic centimeters of wet sediment. For all samples, macrofossil counts included chironomid head capsules, seeds identified to genus, *Daphnia* spp. ephippia, *Cenococcum* sclerotia (fungal resting bodies) and oribatid mites. Qualitative values for the detrital fraction were calculated on a scale of 0-5 corresponding to 0 %, 1-20 %, 21-40%, 41-60%, 61-80 % and 81-100% respectively. Three radiocarbon samples were selected from sediment cores extracted from the centers of Claudi and Jaeger.

Dating was by accelerator mass spectrometry and carried out at The University of California Irvine (Keck Carbon Cycle Program) and the Poznan Radiocarbon Laboratory, Poland. We converted ^{14}C dates to calibrated years BP using the Calib 7.0 program (http://calib.qub.ac.uk/calib/calib.html) and the Intcal13 radiocarbon curve (Reimer et al., 2013).

4. Results

We identified four facies (F): F1, massive silt lacking aquatic macrofossils and other aquatic indicators; F2, interbedded organic silt (0.2 – 1.25 m in thickness); F3, chaotic silt (0.6 – 2.0 m in thickness); and F4, silt rich mud (0.2 – 2 m in thickness) (Fig. 5). Facies identification is based on visual analysis, macrofossils present and biogeochemical characteristics. Transition between facies generally occurs gradually over 15-30 cm. While the stratigraphic order of facies is consistent, we found that not all facies were present at each core. All facies were present in both lakes, however. In general F2 and F3 decreased in thickness towards the lake center, while F4 increased in thickness although this relationship was not linear. Fig. 6 illustrates a subset of macrofossil and biogeochemical data from a central Claudi core retrieved from a baydjerakh top.

4.1 Facies identification

Facies one (F1): massive silt lacking aquatic macrofossils and other aquatic indicators.

The F1 unit consists of massive bluish-grey silt, often containing rootlets and small pieces of terrestrial organic detritus. Black mottles, frequently occur and range in size from 1-> 5 cm in diameter (Fig. 5). Thirteen samples were analyzed for total organic carbon, $\delta^{13}C$, C/N, 10 samples were analyzed for grain size analysis, and 187 samples were analyzed for magnetic susceptibility (Table 2, a subsample of which is shown in Fig. 6). Samples screened for plant remains (n=3) were found to lack discrete macrofossils with the exception of one *Empetrum* seed.

Facies two (F2): Interbedded organic silt facies.

F2 is found directly above F1. When present together with facies 3 (F3, discussed below), F2 is found underneath it. The basal interbedded organic silt facies is characterized by the presence of coarse bands and few fine dark laminations (Fig. 5). Bands and dark laminations are composed mainly of detrital organic material, silt and reworked tephra (Fig. 5). Bands and dark laminations vary in color greatly but are frequently observed to be dark brown to black. The organic fraction of F2 typically contains a combination of well-preserved *Drepanocladus capillifolius* leaves and *Carex* spp. seeds, suggesting input from a shallow water environment with emergent sedges (Janssens, 1983). Bands and laminations vary in width from 1-10 cm and 0.3-1.0 cm, respectively, and have diffuse boundaries. As a unit, F2 reaches a maximum thickness of 1.25 m in our sediment cores. Twenty four samples were analyzed for total organic carbon, $\delta^{13}C$, C/N, 287 samples were analyzed for magnetic susceptibility (Table 2), and 21 samples were analyzed for macrofossil content (Table 3). Measurements of percent total organic carbon (Table 2), range widely and median magnetic susceptibility values are the second highest among sediment facies (Table 2). The macrofossil composition of the basal interbedded organic-silt facies is dominated by *Cenococcum* sclerotia, oribatid mites, and ostracods valves (Table 3, n=21).

Facies three (F3): Chaotic silt facies.

The predominant characteristic of this facies is a massive silt matrix containing occasional peat balls, lenses or distorted bands of Pleistocene and/or Holocene peat, thawed Pleistocene yedoma, and redeposited Devil Mountain tephra (Fig. 5). Inclusions, bands and lenses of peat, silt and tephra vary from <1 cm to approximately 10 cm in thickness or, in the case of silt and tephra, they appear as massive sub-units. Boundaries range from abrupt to diffuse. Tephra inclusions tend to be poorly sorted (based on visual observations) with high magnetic susceptibilities (>50 SI 10^{-6}). This facies has the lowest median %TOC (Table 2, n=14), but higher % TOC values can be seen where large organic inclusions occur (e.g., Fig. 6, 160 cm depth). Median C/N (n=14) and $\delta^{13}C$ (n=14) values are somewhat similar to other facies (Table 2). Median grain size is 28.6 µm, corresponding to silt (n=3) (Table 2). Three hundred and ninety nine samples were measured for magnetic susceptibility (Table 2). The chaotic basal facies can reach a thickness of approximately two meters, though more commonly it is 50 to 90 cm. Terrestrial indicators, such as seeds from *Carex*, *Empetrum* spp. and *Betula* spp. that are characteristic of water-logged alases (Jones et al., 2012) are present within this facies. *Cenococcum* sclerotia and oribatid mites are also common. The coarse (>250 μm) fraction is mainly composed of herbaceous and lignified detritus (Fig. 6, Table 3). Down core analysis of sediment retrieved from a baydjerakh high at Claudi's center exhibited large pieces of graminoid stem, leaves, and rootlets protruding from the organic rich sections of the unit (Fig. 6).

Facies four (F4): silt-rich mud.

F4 is composed of brownish silt often with olive black horizontal laminations with diffuse boundaries. Upper sections of this facies within 10 cm of the sediment-water interface are often less compact than deeper sediments. Upper (0-25 cm) sediment frequently contains shell-fragment horizons of varying thickness. Often, horizontal to sub-horizontal laminations characterize this facies and range in color between brownish black, olive black and black (Fig. 5). Lamination thickness is generally between 0.3-0.9 cm, although the diffuse boundaries make exact width measurements difficult. Smear-slide analysis indicates that dark laminae have a larger fraction of detrital organic matter and a smaller mineral fraction than light laminations. Forty-six samples were analyzed for total organic carbon, C/N and $\delta^{13}C$ (Table 2). Median grain size values are the lowest among sediment units, 22.1 μm, corresponding to silt with a range of 19.38 to 28.32 (n=29), possibly reflecting the highest amount of sorting (Table 2). The median magnetic susceptibility value is the highest among sediment units, 47.2 MS SI 10^{-6} (n=915) (Table 2). The silt-rich mud reaches a maximum thickness of approximately 2 m in our cores.

No aquatic seeds were found within the silt-rich mud, probably because most seeds are deposited close to the lake margin, within the macrophyte zone. Macrofossil composition (n=23) is dominated by ostracods, with small quantities of chironomid head capsules, *Cenococcum* sclerotia, and *Daphnia* spp. ephippia (Table 3). Down core analysis of Claudi Lake's central sediments show numbers of *Cenococcum* sclerotia and *Daphnia* spp. ephippia to decrease down core (Fig. 6).

4.2 Facies distribution within Claudi and Jaeger lakes

Figs. 3 and 4 are schematic representations of the stratigraphies of the transect cores from Claudi and Jaeger, classified according to the four sediment facies described above. The figures also indicate the relation of each core to underwater baydjerakh topography.

4.2.1 Claudi Lake (Fig. 3)

Either F3 or F2 is present at all core locations, and F1 deposits are consistently identified beneath them. The combined thickness of F2 and F3 increase with distance from the lake margin (see section 4.3 below); while F2 thickness ranged from 0.2-1.0 m, those of F3 ranged from 1-2 m. F4 was not present <20 m from the lake margin but increased in thickness from 0.3 to 2 m between 20 and 150 m from the lake margin.

4.2.2 Jaeger Lake (Fig. 4)

F1 deposits are only identified at the lake center and are basal to all other facies. F2 is only present close to the margin (<20 m) in one core (Fig. 4), with a thickness of 0.45 m (based on one observation). F3 is present near the margin and also offshore. F3 thickness ranged from 0.6 - 1.5 m. F4 is present at every location sampled and exhibits a general increase in thickness between the lake margin and lake center, ranging from 0.2 to 0.7 m.

4.3 Relationship between facies thickness and lake margin

To explore the relationship between facies thickness and distance from the margin at Claudi and Jaeger, we evaluated the correlation between distance from the margin and i)

F4 thickness, and ii) the combined thickness of basal facies F2 and F3 (Fig. 7). We used data from fourteen coring locations, each with multiple cores, where sediment accumulated on baydjarakh highs. From observing baydjarakhs in drained lake basin exposures we observed that lows tend to accumulate more sediment than highs, making a direct comparison between the two inappropriate. We found a significant positive correlation between F4 thickness and distance from the margin ($r = 0.73$, $n=7$, $p<0.03$) and a significant negative correlation between thickness of F2 and F3 and distance from the margin ($r = -0.75$, $n=7$, $p<0.02$; Fig. 7). The combined thickness of F2 and F3 ranged from as little as 0 cm at the lake center to ca. 150 cm at the lake margin. F4 thickness ranged from ca. 20 cm at the lake margin to over 200 cm at the lake center. Despite a significant relationship, it should be noted that this data set is based on a small number of samples and can only be considered as a starting point for further exploration of this relationship.

4.4 Radiocarbon dates

To establish the timing of initial lake development for lakes Claudi and Jaeger, we dated herbaceous material and terrestrial leaf fragments from F4 and F3 respectively, close to the lake center (for locations, see Figs. 3, 4). The number of radiocarbon dates are limited due to the prevalence of old carbon within the lake system (Abbott and Stafford Jr, 1996; Oswald et al., 2005). Evidence of old carbon uptake within Claudi lake is seen in the ~2000 yr BP ages of modern day aquatic moss and macrophyte material (Table 4), which precludes dating aquatic plant material. Furthermore, the nature of thermokarsting results in extensive reworking of organic fragments (Hopkins and Kidd, 1988). Terrestrial herbaceous material from a sediment depth of 72 cm in Jaeger Lake yielded an age of 3646-3634 calibrated years BP (all calibrated ages within the 1-sigma, 68%, range). Terrestrial herbaceous material (from a sediment depth of 234 cm) and a terrestrial leaf fragment (from a sediment depth of 166 cm) from Claudi Lake yielded ages of 20,205-

19,939 and 1080-1152 calibrated years BP, respectively (Table 4). The older date from Claudi is assumed to be on reworked Pleistocene material.

5. Discussion

5.1 Sediment facies distribution and depositional environment

Numerical modeling of thermokarst lakes indicates that a talik should exist beneath any lake in permafrost regions where water depth exceeds maximum lake ice thickness (Ling et al. 2003; West and Plug 2008; Kessler et al. 2012). Field observations of sediments associated with taliks are consistent in describing the presence of a taberal facies for yedoma thermokarst lakes (Wetterich 2009; Wetterich 2012, Walter Anthony 2014). We suggest that F1 formed when formerly subaerial permafrost deposits thawed in situ below Claudi and Jaeger lakes, creating taberal deposits. We interpret F1 to be a taberal facies due to a number of factors. F1 is a massive facies, with low levels of organics, consistently located beneath all other facies (Figs. 3, 4, 6). These findings agree with existing definitions of taberal deposits (see Romanovskii et al., 2004; Schirrmeister et al., 2011; Wetterich et al., 2012). The absence of aquatic macrofossils in F1 (Table 3) suggests an original terrestrial depositional environment, while the lack of sedimentary and cryolithological structures, suggests post depositional diagenesis via thaw and compaction.

Low quantities of other macrofossil remains within F1 may relate to any or all of the following: 1) the small volume of sediment analyzed (n=7, compared to between 18 and 45 samples for other facies), 2) generally low concentrations of discrete macrofossils within the original yedoma deposits, or 3) the intense decomposition of macrofossils in a sub-lake talik over long time. Walter Anthony et al. (2014) found mainly detrital and graminoid material in macrofossil analyses of taberal sediments beneath tens of yedoma lakes in Siberia. The remains found in this study are also largely herbaceous, although lignified material is also present. The ~28% lower percent organic carbon in taberal sediments vs. undisturbed yedoma in Siberia (Walter Anthony et al., 2014) supports our conclusion that intense decomposition of yedoma beneath the lake leads to a paucity of identifiable macrofossils.

Above F1, the basal deposits (F2, F3) consistently occur. These provide a transition between F1 and F4 (silt-rich lake mud; Figs. 3, 4). F2 is dominated by terrestrial indicators. Within F2, seeds from plants that inhabit lake shore environments (*Pontentilla palustris*), shallow lake margin areas (*Hippurus* spp.), terrestrial slopes and yedoma uplands (*Carex* trigonal, *Carex* lenticular, *Empetrum* spp.) are all present, indicating deposition at a lake-margin or in a shallow pond. We interpret F2 to represent the sorting of coarse detrital material at the lake margins via summer wave energy when the lake is not frozen. Alternating beds of silt, tephra and detrital organics suggest that material entering the lake via thaw and collapse is retransported, sorted and redeposited in layers by wave action at the lake margin (as described by Hopkins and Kidd, 1988; Murton, 2001). We propose that the development of F2 relies on the presence of a shallow shelf adjacent to the lake margin, facilitating reworking of material by wave winnowing. While conducting fieldwork at Claudi Lake during the summer of 2010 we observed bluff material that had slumped down adjacent to the lake margin, which was subsequently being reworked by wave action.

Prevailing winds from the north (Western Regional Climate Center, www.wrcc.dri.edu, 09/01/15) largely control the direction of surface currents within lake systems (Wetzel, 2001). Therefore, it is likely that the prevailing wind direction affects the spatial distribution of F2 around the lake margin. Marginal sections of the lake receiving the highest energy and most frequent wave action are probably more susceptible to bank erosion and sorting of material.

We interpret F3 to represent a marginal depositional environment where the dominant process is the thaw and slump of bank material. Another possible mechanism responsible for the development of F3 is the distortion of F1 due to continuing subsidence and thaw of excess ice as the lake expands. Evidence of this process in the form of basal sediment faulting has been described for thermokarst lakes on the Tuktoyaktuk Peninsula (Murton, 1996). Similarly, Andreev et al. (2009) describe faulting and slumping of lacustrine sediments along the margins of ice wedge casts studied in a North Siberian coastal bluff exposing early Holocene thermokarst lake sediments. Although F3 lacks aquatic seeds, it does contain high numbers of both ostracodes and chironomid head capsules (Table 3). The absence of aquatic seeds may be due to high sedimentation rates in margin areas of F3 formation that may prevent the establishment of aquatic plants such as *Hippurus* spp. and *Potomageton* spp. or indeed overwhelm any aquatic production with large amounts of terrestrial material.

On the Seward Peninsula, both F2 and F3 contain reworked tephra from the Devil Mountain Maar eruption (Begét et al., 1996). Within F2 and F3, tephra inclusions and layers represent reworked material and directly correlate with high magnetic susceptibility (see Fig. 6). Large grain size is also evident within deposits containing tephra. The lack of cohesion exhibited by the coarse-grained tephra after thawing in the bluffs may exacerbate the bank slumping in our study lakes.

Silt-rich mud, F4, formed within deeper, calmer waters where fine material is able to settle out of suspension. The presence of F4 within 20 m of both Claudi and Jaeger's upland margin (Figs. 3, 4) suggests that a depositional environment characterized by fine-grained, slower sedimentation develops relatively quickly following margin expansion. Ostracodes and chironomid head capsules (aquatic macrofossils) dominate F4 (Table 3). Terrestrial macrofossils are less abundant in F4 than in F2 and F3. This is likely due to most discrete terrestrial macrofossils being deposited closer to the margin. Laminations reflect variability in minerogenic input and are likely related to discrete episodes of bank collapse in which large amounts of silt are released; these settle out faster than organic fines.

5.2 Timing of lake development

Given the potential for old carbon (Pleistocene-aged) contamination within Arctic lake systems (Abbott and Stafford Jr, 1996; Oswald et al., 2005) it is important to assess the accuracy of our radiocarbon dates. Given Jaeger Lake's radius is 365 m, and assuming radial expansion, the 3646-3634 calibrated years BP age would yield a mean expansion rate of 0.10 m/yr. This is similar to modern expansion rates observed for upland margins of first-generation thermokarst lake in our study area (0.18 m/yr; Jones et al., 2011). Given Claudi's radius of 288 m, and assuming radial expansion, the younger age of 1080-1152 calibrated years BP would yield a mean an expansion rate of 0.25 m/yr (Jones et al., 2011). Taking into consideration that modern day rates for Claudi Lake range from 0.1 to >0.5 m/yr, this age is a reasonable basal age.

Lake expansion rates are not necessarily linear over time. Smaller, younger upland lakes tend to be less deep and therefore there is less material to be mobilized along banks for expansion to take place, resulting in relatively high initial expansion rates. On the Seward Peninsula small upland lakes exhibit expansion rates as high as 2 m/yr (Jones et al., 2011). Therefore both Jaeger and Claudi likely expanded at faster rates during early stages of development. Once both subaerial and subaqueous bluff height increased and total sediment volume to be removed from eroding bluffs became higher, expansion rates would have slowed and sedimentation rates at the basin centers would also have slowed.

5.3 Comparison with previous studies on yedoma thermokarst lakes

While previous work by Murton (1992) conducted high-resolution sedimentological analysis on drained lake basins, these lakes were formed within glacial outwash and till in the North West Territories, Canada. Our study therefore presents the first cross-basin analysis of an existing thermokarst lake and one forming within yedoma sediments.

Our data corroborate and refine previous observations on northern Seward Peninsula yedoma thermokarst lakes (e.g., Hopkins and Kidd, 1988). Hopkins and Kidd (1988) identified both a sandy, organic-rich detrital basal unit and an overlying unit of fine-grained, bedded sediment similar to our basal facies (F2 and F3) and to F4, respectively. The main difference we identified was that basal deposits vary enough visually to be divided into two sub-facies, instead of a single basal facies.

In the Brooks Range Foothills, Alaska, Rawlinson (1990, his Fig. 5.5) identified two generations of thermokarst lakes in exposures that formed within yedoma-like sediment. The facies described are similar to those we have identified in this study (Table 2). First-generation lake sediment is described as organic silt, which we interpreted as possibly similar to F4. Rawlinson (1990) also noted that ice wedge pseudomorphs (baydjerakh lows) influence sediment distribution.

In northeastern Siberia, drained yedoma thermokarst lake exposures containing facies similar to those identified within this study are described (Wetterich et al., 2009). Wetterich et al. (2009) identify a massive grey silt which they interpret to be taberal deposits, similar to F1 in this study. Also described are ice wedge casts characterized by alternating beds of peaty detrital layers and grey clay-silt layers, visually similar to F2. In the Lena River Lowlands, yedoma thermokarst lakes contain a sediment facies most similar to F4 (Biskaborn et al., 2013). A single core was analyzed from a yedoma thermokarst lake in the Lena River lowlands; this was composed of clayey silt with fine layers of sand and organics, exhibiting similar visual characteristics to F4 identified in this study.

Walter Anthony et al. (2014) identified a suite of facies from 49 drained lake basin exposures in NE Siberia. Overall, the stratigraphic pattern they observed was similar to this study: a taberal unit overlain by an organic rich basal unit and an organic rich fine-grained unit. One difference is that these authors combined the basal interbedded organic-silt facies (F2, this paper) and chaotic basal facies (F3 this paper) into a single facies, which they termed 'Lacustrine silt'.

One key difference between lake deposits on the northern Seward Peninsula and other regions is the presence of volcanic tephra. As suggested above, the presence of coarse grained, ice-rich tephra layers may result in particularly unstable marginal scarps. Due to the larger grain size of tephra it lacks shear strength; this may lead to material being more susceptible to erosion and lake expansion being particularly rapid, and to dominance of the chaotic basal facies (F3 is the most common facies in our study).

5.4 Conceptual model of lake development

We identified three subaqueous depositional environments: a high-energy margin environment dominated by wave action responsible for the formation of F2, a high-energy margin environment dominated by bank thaw and collapse events responsible for the formation of F3 and a low-energy central basin environment dominated by sediment settling where F4 forms. Despite being deposited subaerially to form yedoma, the characteristics of F1 are shaped by post-depositional processes (thaw, compaction and distortion).

Models of thermokarst lake development suggest lake initiation at a central point followed by continued margin expansion and vertical settlement (Hopkins and Kidd, 1988; Kessler et al., 2012). We found the distribution of facies and the corresponding depositional environments within Claudi and Jaeger Lakes to support these models (Figs. 3, 4). At all coring locations across Claudi Lake, F4 was underlain by either F2 or F3, which we suggest forms in margin environments. We also observed a positive relationship between F4 thickness and distance from the lake margin (Fig. 7) possibly due to a longer period of F4 sediment accumulation in central areas of the lake basin. We suggest that the presence of baydjerakhs and flat lake bottom inhibit any significant sediment focusing.

In order to create a conceptual model of lake development we first considered how our data fit within existing frameworks of thermokarst dynamics (e.g. Billings and Peterson, 1980; Hopkins and Kidd 1988; Murton, 1996; Jorgenson and Shur, 2007; Wetterich et al. 2012, Morgenstern et al., 2013). With these existing frameworks in mind we then combined the sedimentology of Claudi Lake with field-based morphological descriptions (Soloviev, 1973; 1980; Burn, 1992; Grosse et al., 2013; Morgenstern et al., 2013), and observed spatial dynamics of thermokarst lakes in our study area (Jones et al., 2011).

Thermokarst processes are initially triggered by a disturbance to the ground thermal regime (Burn and Smith, 1990; Murton, 2009) (Fig. 8A). Subsequently the first stage of lake development begins with the thaw of excess ice, collapse of the ground surface, and flooding of the formerly subaerial surface (Burn, 1992; Grosse et al., 2013), leading to the formation of F2 and the initiation of baydjerakh topography (Hopkins and Kidd 1988) (Fig. 8B). At this early stage of development, no other facies are present.

In the second stage (Fig. 8C), vertical subsidence and lateral erosion deepen the lake (Kessler et al., 2012). Subsidence, currents, and seasonal sediment freeze-thaw processes may deform or rework F2 deposits, which may result in the formation of F3. Once subsidence has advanced to where lake depth is greater than maximum winter ice thickness (Jones et al., 2009; Arp et al., 2010), F1 (talik) forms beneath the lake (West and Plug, 2008; Ling et al., 2012). During stage two, a central lake basin becomes established and F4 begins to accumulate.

During the third stage of development (Fig. 8D), lake-bottom baydjarakh topography becomes more pronounced as ice-wedge thaw progresses downwards (Soloviev, 1962). Marginal bluff height increases, causing bank thaw and collapse and the continued formation of F3. The reworking by wave action of material from F3 at the lake margin (Hopkins and Kidd, 1988; Murton, 2001) results in continued deposition of F2. As horizontal expansion by thaw and collapse and vertical subsidence due to thaw continues to occur (Kessler et al., 2012), further deformation of sediment below the sub-lacustrine unconformity occurs due to thaw compaction, and F1 thickens. F4 continues to accumulate in the center of the lake and also towards the lake margin. While F4 exhibits thinning towards the lake margin, F2 and F3 exhibit thickening because of continued slumping and reworking, as well as increasing marginal bluff height as subsidence advances (Hopkins and Kidd, 1988; Plug and West, 2009). We found this relationship to be more evident in Claudi Lake than Jaeger Lake although this may be due to higher core sampling density at Claudi Lake. The combined thickness of F2 and F3 at Claudi Lake's center was more than 1 m thicker than at the margin while similar thicknesses at both the margin and center were observed in Jaeger Lake (Figs. 3, 4).

In the final stage of lake development (Fig. 8E) excess ice becomes completely depleted beneath the lake center (West and Plug, 2008; Plug and West, 2009), and thaw subsidence ceases. At the lake margin thaw and subsidence continues with ongoing lake expansion, maintaining baydjerakh topography. The lake bottom begins to flatten in the ground ice-depleted center (Plug and West 2009) where baydjerakh lows begin to infill with F4 (Hopkins and Kidd, 1988) (Fig.3).

Our interpretations for thermokarst lake facies evolution in ice-rich permafrost on the Seward Peninsula provide a foundation from which to explore yedoma thermokarst lake development and sedimentology, and for comparison with thermokarst lake evolution in different permafrost types. Numerous factors may cause variation in facies development. Sediment distribution patterns and thickness may vary due to the specific baydjarakh and trough configuration (and the spatial distribution of ground ice prior to thermokarst initiation), causing very local highs and lows in the bathymetry of these lakes. Lake drainage events may cause variations in sediment distribution. Partial drainage may occur gradually or catastrophically (Jones et al., 2011; Grosse et al., 2013) and may cause the full or partial removal of F2, F3 and F4. Partial drainage is evident at Claudi in the form of an inactive drainage channel located at the north margin and in Jaeger in the form of an active channel at the NW margin; however, this event was not clearly recorded in either lake's sediment record. Sedimentology may also be affected by the drainage of adjacent lake basins. If drainage of an adjacent lake is diverted into the lake basin this may result in the addition of sediment and water to the lake system.

The rate at which lake expansion and the development of F2 and F3 occurs is complicated by bank retreat. This is regulated by how rapidly material is removed from thawing banks and transported into the lake (Kessler et al., 2012). Until in situ thawed bank material is removed from the lake bluff, it insulates underlying frozen material from further thaw, thereby slowing margin retreat. Thermokarst lake coalescence may also affect facies distribution via erosion and transportation of lake sediment. Numerical modeling of Claudi Lake's formation suggests that it formed from the coalescence of two smaller lakes (Kessler et al., 2012). Jaeger Lake's hourglass shape may also be due to the coalescence of two lakes.

The thickness of F1 (talik development) also depends on a number of factors that vary within and among thermokarst lake regions. Thermal conductivity of material below the lake depends on lithological and permafrost properties. Heat transfer from the lake water into the thaw bulb depends mainly on the average lake bed temperature, substrate density and ice density (Kessler et al., 2012). Thaw bulb development is initially rapid, but slows as thickening thawed material begins to insulate underlying permafrost and heat has to be transferred through more material.

Estimating the rates of lake development from initiation to drainage is challenging, as it is likely to be a non-linear process. Further work investigating lake initiation and initial expansion are needed to establish a solid chronology of lake development.

6. Conclusions

This study illustrates the spatially and temporally dynamic nature of yedoma thermokarst lake depositional environments. Four sedimentary facies are present in first-generation yedoma thermokarst lakes on the northern Seward Peninsula, and at any given location in a lake, these facies shift as first-generation lakes evolve. The facies identified represent three main depositional environments (F2, F3, F4) and a zone of subaquatic deformation of former terrestrial permafrost deposits (F1) beneath the lake due to thaw and compression. F2 deposits form in high-energy margin environments, where wave processes rework detrital organic material and tephra. F3 deposits represent a high-energy margin environment where bank thaw and collapse causes the accumulation and burial of silt, organic detritus and tephra. F4 deposits represent a low energy depositional environment towards the lake center where fine grained material can settle out of suspension.

The sequence of facies identified provides a clear picture of the spatial expansion pattern of a yedoma thermokarst lake. F2 and F3 are basal deposits, and at least one is always present beneath F4. The existence of F2 and F3 across both Claudi and Jaeger support the theory that thermokarst lakes have time-transgressive margins that are continually eroding.

There are strong similarities between the northern Seward Peninsula facies and sediment sequences described in other yedoma lakes in both Alaska and northeast Siberia. Similarities are primarily the visual characteristics of facies present. The presence of tephra in Seward Peninsula yedoma thermokarst lakes appears to be unique to the region and may influence the relative importance of certain facies types.

Our model of lake facies distribution and their organic carbon contents provide an important component needed to quantify carbon budgets in Alaskan and Siberian permafrost regions. Data from this study complements estimates of total organic carbon within drained lake basin peats (Jones et al., 2012; Walter Anthony et al., 2014), upland yedoma deposits (Strauss et al., 2013), as well as measurements of thermokarst lake methane emissions (Walter et al., 2007b), and modeled thaw bulb dimensions (West and Plug, 2008; Kessler et al., 2012).

These results help improve field identification of yedoma thermokarst lake deposits in the periglacial sedimentary record and allow better interpretation of the depositional regime present in a given thermokarst lake sediment exposure or core. In turn, this will enhance our ability to reconstruct Holocene landscape evolution in Arctic and sub-Arctic lowlands.

Acknowledgements

We thank Laura Oxtoby, Laurel McFadden, Ben Jones, and Peter Anthony for help with field and lab work. Funding for this study was provided through NSF grant ARC-0732735. Any opinions, findings, conclusions, or recommendations expressed in this material are those of the authors and do not necessarily represent the views of the National Science Foundation. We thank the US National Park Service for permission to do work within the Bering Land Bridge National Preserve. We thank researchers at LacCore for assistance and use of laboratory facilities. This manuscript has benefited from reviews by D. Mann, J. Begét and two anonymous reviewers.

References

Abbott, M.B., Stafford Jr, T.W., 1996. Radiocarbon geochemistry of modern and ancient arctic lake systems, Baffin Island, Canada. Quaternary Research 45, 300–311.

Andreev, A.A., Grosse, G., Schirrmeister, L., Kuznetsove, T.V., Kuzmina, S.A., Bobrov, A.A., Tarasov, P.E., Novenko, E.Y., Meyer, H., Derevyagin, A.Y., Kienast, F., Bryantseva, A., Kunitsky, 2009. Weichselian and Holocene palaeoenvironmental history of the Bol'shoy Lyakhovsky Island, New Siberian Archipelago, Arctic Siberia. Boreas 38, 72–110.

Arp, C.D., Jones, B.M., 2009. Geography of Alaska lake districts: identification, description, and analysis of lake-rich regions of a diverse and dynamic state. U.S. Geological Survey Scientific Investigations Report 2008–5215, (40 pp.).

Arp, C.D., Jones, B.M., Whitman, M., Larsen, A., Urban, F.E., 2010. Lake temperature and ice cover regimes in the Alaskan subarctic and arctic: Integrated monitoring, remote sensing, and modeling. Journal of the American Water Resources Association 46, 777–791.

Begét, J.E., Hopkins, D.M., Charron, S.D., 1996. The largest known maars on Earth, Seward Peninsula, northwest Alaska. Arctic 49, 62-69.

Billings, W.D., Peterson, K.M., 1980. Vegetational change and ice-wedge polygons through the thaw-lake cycle in Arctic Alaska. Arctic and Alpine Research 12, 413-432.

Birks, H., 2002. Plant Macrofossils. In: Smol, J.P., Birks, H.J., Last, W.M. (Eds.), Tracking Environmental Change Using Lake Sediments. Volume 3: Terrestrial, algal and silicious indicators. Kluwer Academic Publications, NY, USA, pp. 49-74.

Biskaborn, B.K., Herzschuh, U., Bolshiyanov, D.Y., Schwamborn, G., Diekmann, B., 2013. Thermokarst processes and depositional events in a tundra lake, northeastern Siberia. Permafrost and Periglacial Processes 24, 160-174.

Brosius, L.S., Walter Anthony, K.M., Grosse, G., Chanton, J.P., Farquharson, L.M., Overduin, P.P., Meyer, H., 2012. Using the deuterium isotope composition of permafrost meltwater to constrain thermokarst lake contributions to atmospheric CH_4 during the last deglaciation. Journal of Geophysical Research 117, G01022, DOI:10.1029/2011JG001810

Burn, C.R., 1992. Thermokarst lakes. The Canadian Geographer 36, 81–85.

Burn, C.R., Lewkowicz, A.G., 1990. Retrogressive thaw slumps. The Canadian Geographer 34, 273–276.

Burn, C.R., Smith, M.W., 1990. Development of thermokarst lakes during the Holocene at sites near Mayo, Yukon Territory. Permafrost and Periglacial Processes 1, 161–175.

Charron, S.D., 1995. Surficial mapping of the Cape Espenberg-Devil Mountain region and lake core analyses from North Killeak Lake, Bering Land Bridge National Preserve, western Alaska. MSc Thesis, University of Massachusetts, MA, USA.

Côté, M.M., Burn, C.R., 2002. The oriented lakes of Tuktoyaktuk Peninsula, western arctic coast, Canada: a GIS-based analysis. Permafrost and Periglacial Processes 13, 61–70.

Czudek, T., Demek, J., 1970. Thermokarst in Siberia and its influence on the development of lowland relief. Quaternary Research 1, 103–120.

French, H. 1996. The Periglacial Environment 2nd ed.Wiley, Hoboken, NJ 478 pp.

Godin, E., Fortier, D., 2012. Geomorphology of a thermo-erosion gully, Bylot Island, Nunavut, Canada. Canadian Journal of Earth Sciences 49, 979–986.

Goetcheus, V.G., Birks, H., 2001. Full-glacial upland tundra vegetation preserved under tephra in the Beringia National Park, Seward Peninsula, Alaska. Quaternary Science Reviews 20, 135–147.

Grosse, G., Jones, B., Arp, C., 2013. Thermokarst lakes, drainage, and drained basins. In Treatise on Geomorphology. In: French, H., Harbor, J. (Eds.), Treatise on Geomorphology. Volume 8: Glacial and Periglacial Geomorphology. Academic Press, San Diego, CA, USA, pp. 325–353.

Hinkel, K., Eisner, W.R., Bockheim, J.G., Nelson, F.E., Peterson, K.M., Dai, X.Y., 2003. Spatial extent, age, and carbon stocks in drained thaw lake basins on the Barrow Peninsula, Alaska. Arctic Antarctic and Alpine Research 35, 291–300.

Hinkel, K.M., Frohn, R.C., Nelson, F.E., Eisner, W.R., Beck, R.A., 2005. Morphometric and spatial analysis of thaw lakes and drained thaw lake basins in the western Arctic Coastal Plain, Alaska. Permafrost and Periglacial Processes 16, 327–341.

Höfle, C., Ping, C.L., 1996. Properties and soil development of late-pleistocene paleosols from Seward Peninsula, Northwest Alaska. Geoderma 71, 219–243.

Höfle, C., Edwards, M.E., Hopkins, D.M., Mann, D.H., 2000. The full-glacial environment of the northern Seward Peninsula, Alaska, reconstructed from the 21,500-year-old Kitluk paleosol. Quaternary Research 53, 143–153.

Hopkins, D.M., Kidd, J., 1988. Thaw lake sediments and sedimentary environments. In: Senneset, K. (Ed.), Fifth International Conference on Permafrost. Tapir Publishers, Trondheim, Norway, pp. 790–795.

Hubberten, H.W., Romanovskii, N.N., 2003. The main features of permafrost in the Laptev Sea region, Russia - a review. In: Heaberli, W., Brandova, D. (Eds.), Eighth International Conference on Permafrost. Zurich, Switzerland, pp. 431–436.

Ireland, R.R., 1982. Moss flora of the maritime provinces. National Museums of Canada, National Museum of the Natural Sciences, Ottawa 738 pp..

Jiilavenkatesa, A., Dapkunas, S.J., Lum, L.H., 2001. Chapter 6: Size characterization by laser light diffraction techniques. In: Jiilavenkatesa, A., Dapkunas, S.J., Lum, L.H. (Eds.), Particle Size Characterization. National Institute of Standards Technology, Technology Administration, U.S. Department of Commerce. Special publication 960-1, pp. 7-25.

Jones, B.M., Arp, C.D., Hinkel, K.M., Beck, R.A., Schmutz, J.A., Winston, B., 2009. Arctic lake physical processes and regimes with implications for winter water availability and management in the National Petroleum Reserve Alaska. Environmental Management 43, 1071–1084.

Jones, B.M., Grosse, G., Arp, C.D., Jones, M.C., Walter Anthony, K., Romanovsky, V.E., 2011. Modern thermokarst lake dynamics in the continuous permafrost zone, northern Seward Peninsula, Alaska. Journal of Geophysical Research, 116, G00M03, doi:10.1029/2011JG001666

Jones, M.C., Grosse, G., Jones, B.M.,Walter Anthony, K., 2012. Peat accumulation in drained thermokarst lake basins in continuous, ice-rich permafrost, northern Seward Peninsula, Alaska. Journal of Geophysical Research, 117, G00M07, doi:10.1029/2011JG001766

Jorgenson, M.T., Osterkamp, T.E., 2005. Response of boreal ecosystems to varying modes of permafrost degradation. Canadian Journal of Forest Research 35, 2100–2111.

Jorgenson, M.T., Shur, Y. 2007. Evolution of lakes and basins in northern Alaska and discussion of the thaw lake cycle. Journal of Geophysical Research, 112, F02S17, doi:10.1029/2006JF000531.

Jorgenson, M.T., Shur, Y.L., Pullman, E.R., 2006. Abrupt increase in permafrost degradation in Arctic Alaska. Geophysical Research Letters, 33, L02503, doi:10.1029/2005GL024960.

Jorgenson, M.T., Shur, Y.L., Osterkamp, T.E., 2008. Thermokarst in Alaska. In: Kane, D.L., Hinkel, K.M. (Eds.). Ninth International Conference on Permafrost. Fairbanks, Alaska: Institute of Northern Engineering, University of Alaska Fairbanks, AK, USA, pp. 869–876.

Jorgenson, M.T., Yoshikawa, K., Kanevskiy, M., Shur, Y., Romanovsky, V.E., Marchenko, S., Grosse, G., Brown, J., Jones, B., 2008. Permafrost Characteristics of Alaska – A new permafrost map of Alaska (map). In: D. L. Kane, K. M. Hinkel, (Eds.).

Ninth International Conference on Permafrost. Fairbanks, Alaska: Institute of Northern Engineering, University of Alaska Fairbanks, AK, USA, pp. 121-122.

Kanevskiy, M., Shur, Y., Fortier, D., Jorgenson, M.T., Stephani, E., 2011. Cryostratigraphy of late Pleistocene syngenetic permafrost (yedoma) in northern Alaska, Itkillik River exposure. Quaternary Research 75, 584–596.

Katamura, F., Fukuda, M., Bosikov, N.P., Desyatkin, R. V, Nakamura, T., Moriizumi, J., 2006. Thermokarst formation and vegetation dynamics inferred from a palynological study in Central Yakutia, Eastern Siberia, Russia. Arctic Antarctic and Alpine Research 38, 561–570.

Katz, J., Katz, S.V., Kipiani, G., 1965. Atlas and keys of fruits and seeds occurring in the Quaternary deposits of the USSR, Commissions for Investiagations of the Quaternary Period, Nauka, Moscow, 367 pp.

Kessler, M.A., Plug, L.J., Walter Anthony, K.M., 2012. Simulating the decadal- to millennial-scale dynamics of morphology and sequestered carbon mobilization of two thermokarst lakes in NW Alaska. Journal of Geophysical Research 117, G00M06, doi:10.1029/2011JG001796.

Kuzmina, S., Elias, S., Matheus, P., Storer, J.E., Sher, A., 2008. Paleoenvironmental reconstruction of the Last Glacial Maximum, inferred from insect fossils from a tephra buried soil at Tempest Lake, Seward Peninsula, Alaska. Palaeogeography, Palaeoclimatology, Palaeoecology 267, 245–255.

Ling, F., Wu, Q., Zhang, T., Niu, F., 2012. Modelling open-talik formation and permafrost lateral thaw under a thermokarst lake, Beiluhe Basin, Qinghai-Tibet Plateau. Permafrost and Periglacial Processes 23, 312–321.

Livingstone, D.A., 1954. On the orientation of lake basins. American Journal of Science 252, 547–554.

Mackay, J.R., 1988. Catastrophic lake drainage, Tuktoyaktuk Peninsula area, District of Mackenzie. Current Research, Current Research Part D, Geological Survey Canada, pp. 83-90.

Mann, D.H., Groves, P., Reanier, R.E., Kunz, M.L., 2010. Floodplains, permafrost, cottonwood trees, and peat: What happened the last time climate warmed suddenly in arctic Alaska? Quaternary Science Reviews 29, 3812-3830.

Marsh, P., Russell, M., Pohl, S., Haywood, H., Onclin, C., 2009. Changes in thaw lake drainage in the Western Canadian Arctic from 1950 to 2000. Hydrological Processes 23, 145–158.

Morgenstern, A., Grosse, G., Günther, F., Fedorova, I., Schirrmeister, L., 2011. Spatial analyses of thermokarst lakes and basins in Yedoma landscapes of the Lena Delta. The Cryosphere Discussions 5, 1495–1545.

Morgenstern, A., Ulrich, M., Günther, F., Roessler, S., Fedorova, I. V., Rudaya, N.A., Wetterich, S., Boike, J., Schirrmeister, L., 2013. Evolution of thermokarst in East Siberian ice-rich permafrost: A case study. Geomorphology 201, 363–379.

Murton, J.B., 1996. Thermokarst-lake-basin sediments, Tuktoyaktuk Coastlands, western Arctic Canada. Sedimentology 43, 737–760.

Murton, J.B., 2001. Thermokarst sediments and sedimentary structures, Tuktoyuktuk Coastlands, western Arctic Canada. Global and Planetary Change 28, 175-192.

Murton, J.B. 2009., Global warming and thermokarst. In: Margesin R. (Ed.), Permafrost Soils. Springer, Berlin Heidelberg, pp. 185–203.

Osterkamp, T.E., Viereck, L., Shur, Y., Jorgenson, M.T., Racine, C., Doyle, A., Boone, R.D., 2000. Observations of thermokarst and its impact on boreal forests in Alaska, USA. Arctic Antarctic and Alpine Research 32, 303–315.

Oswald, W.W., Anderson, P.M., Brown, T.A., Brubaker, L.B., Hu, F.S., Lozhkin, A.V., Tinner, W., Kaltenrieder, P., 2005. Effects of sample mass and macrofossil type on radiocarbon dating of arctic and boreal lake sediments. The Holocene 15, 758–767.
Plug, L.J., West, J.J., 2009. Thaw lake expansion in a two-dimensional coupled model of heat transfer, thaw subsidence, and mass movement. Journal of Geophysical Research-Earth Surface 114, F01002, doi:10.1029/2006JF000740.

Plug, L.J., West, J.J., 2009. Thaw lake expansion in a two-dimensional coupled model of heat transfer, thaw subsidence, and mass movement, Journal of Geophysical Research, 114, F01002, doi:10.1029/2006JF000740.

Rawlinson, S.E., 1990. Surficial Geology and Morphology of the Alaskan central Arctic Coastal Plain, Fairbanks. Alaska Division of Geological and Geophysical Surveys Public Data File 90-27, 326 pp.

Reasoner, M.A., 1993. Equipment and procedure improvements for a lightweight, inexpensive, percussion core sampling system. Journal of Paleolimnology 8, 273–281.

Regmi, P., Grosse, G., Jones, M.C., Jones, B.M., Anthony, K.W., 2012. Characterizing post-drainage succession in thermokarst lake basins on the Seward Peninsula, Alaska with TerraSAR-X backscatter and Landsat-based NDVI data. Remote Sensing 4, 3741–3765.

Reimer, P., Bard, E., Bayliss, A., Beck, W., Blackwell, P.G., Bronk Ramsey, C.E.B., Cheng, H., Edwards, R.L., Friedrich, M., Grootes, P.M., Guilderson, T.P., Haflidason, H., Hajdas, I., Hatté, C., Heaton, T.J., Hoffmann, D.L., Hogg, A.G., Hughen, K.A., Kaiser, K.F., Kromer, B., Manning, S.W., Niu, M., Reimer, R.W., Richards, D.A., Scott, E.M., Southon, J.R., Staff, R.A., Turney, C.S.M., van der Plicht, J., 2013. IntCal13 and Marine13 radiocarbon age calibration curves 0–50,000 years cal BP. Radiocarbon 55, 1869–1887.

Romanovskii, N.N., Hubberten, H.W., Gavrilov, A.V., Tumskoy, V.E., Kholodov, A.L., 2004. Permafrost of east Siberian Arctic shelf and coastal lowlands. Quaternary Science Reviews 23, 1359-1369.

Schirrmeister, L., Grosse, G., Wetterich, S., Overduin, P., Strauss, J., Schuur, E.A.G., Hubberten, H.W., 2011. Fossil organic matter characteristics in permafrost deposits of the northeast Siberian Arctic. Journal of Geophysical Research 116, G00M02, doi:10.1029/2011JG001647.

Schirrmeister, L., Froese, D.G., Tumskoy, V., Grosse, G., Wetterich, S., 2013. Yedoma: Late Pleistocene ice-rich syngenetic permafrost of Beringia. In: Elias, S. (Ed.), Encyclopedia of Quaternary Science. Elsevier, Amsterdam, pp. 542 – 552.

Schnurrenberger, D., Russell, J., Kelts, K., 2003. Classification of lacustrine sediments based on sedimentary components. Journal of Paleolimnology 29, 141–154.

Soloviev, P.A., 1962. Alas relief of Central Yakutia and its origin Territory. In Permafrost and accompanying phenomena on the territory of the Yakutian ASSR. USSR Academy of Sciences, Moscow pp. 38–53. (In Russian)

Soloviev, P.A., 1973. Thermokarst phenomena and landforms due to frost heaving in Central Yakutia. Biuletyn Peryglacjalny 23, 135–155.

Strauss, J., Schirrmeister, L., Grosse, G., Wetterich, S., Ulrich, M., Herzschuh, U., Hubberten, H.W., 2013. The deep permafrost carbon pool of the Yedoma region in Siberia and Alaska. Geophysical Research Letters 40, 6165–6170, doi:10.1002/2013GL058088.

Van Everdingen, R.O., 1988. Multi-language glossary of permafrost and related ground-ice terms, Boulder, CO: National Snow and Ice Data Center/World Data Center for Glaciology. Available at https://nsidc.org/fgdc/glossary/.

Walter Anthony, K.M., Anthony, P., 2013. Constraining spatial variability of methane ebullition seeps in thermokarst lakes using point process models. Journal of Geophysical Research: Biogeosciences 118, 1015–1034. doi: /10.1002/jgrg.20087.

Walter Anthony, K.M., Zimov, S.A., Grosse, G., Jones, M.C., Anthony, P., Chapin III, F.S., Finlay, J.C., Mack, M.C., Davydov, S., Frenzel, P., Frolking, S., 2014. A shift of thermokarst lakes from carbon sources to sinks during the Holocene epoch. Nature 511, 452–456.

Walter, K.M., Edwards, M.E., Grosse, G., Zimov, S.A., Chapin, F.S., 2007a. Thermokarst lakes as a source of atmospheric CH_4 during the last deglaciation. Science 318, 633–636.

Walter, K.M., Smith, L.C., Chapin, F.S., 2007b. Methane bubbling from northern lakes: present and future contributions to the global methane budget. Philosophical transactions of the Royal Society London, Series A, Mathematical, physical, and engineering sciences 365 : 1657–1676.

West, J.J., Plug, L.J., 2008. Time-dependent morphology of thaw lakes and taliks in deep and shallow ground ice. Journal of Geophysical Research 113, doi:10.1029/2006JF000696.

Western Regional Climate Center, http://www.wrcc.dri.edu.

Wetterich, S., Schirrmeister, L., Andreev, A., Pudenz, M., Plessen, B., Meyer, H., Kunitsky, V., 2009. Eemian and Late Glacial/Holocene palaeoenvironmental records from permafrost sequences at the Dmitry Laptev Strait (NE Siberia, Russia). Palaeogeography Palaeoclimatology Palaeoecology 279, 73–95.

Wetterich, S., Grosse, G., Schirrmeister, L., Andreev, A.A., Bobrov, A.A., Kienast, F., Bigelow, N.H., Edwards, M.E., 2012. Late Quaternary environmental and landscape dynamics revealed by a pingo sequence on the northern Seward Peninsula, Alaska. Quaternary Science Reviews 39, 26–44.

Wetzel, R.G. 2001., Limnology: Lake and River Ecosystems, Third Edition. Academic Press, New York.

Wolfe, B.B., Edwards, T.W.D., Elgood, R.J., Buening, K.R., 2001. Carbon and oxygen isotope analysis of lake sediment cellulose: methods and applications. In: Last, W.M., Smol, J.P. (Eds.), Tracking Environmental Change Using Lake Sediments. Volume 2: Physical and geochemical methods. Kluwer Academic Publishers, NY, USA, pp. 373–400.

Wright, H.E., Mann, D.H., Glaser, P.H., 1984. Piston corers for peat and lake sediments. Ecology 65, 657–659.

Yoshikawa, K., 2003. Shrinking thermokarst ponds and groundwater dynamics in discontinuous permafrost near council, Alaska. Permafrost and Periglacial Processes 14, 151–160.

Table Captions

Table 1. Basic characteristics of the two lakes studied. Lake area values are based on Ikonos imagery obtained in the summer of 2006. The maximum depths are those measured during field campaigns.

Table 2. Median values for % TOC, C/N, $\delta^{13}C$, and MS and mean values (indicated by an asterisk) for grain size of facies identified. No mean values or standard deviations are stated for % TOC, C/N, $\delta^{13}C$, and MS as data were not found to have a normal distribution.

Table 3. Macrofossils analysis by facies. (A) Quantitative values. The mean number of discrete macrofossils per 7 cc, by sediment facies. Macrofossil counts were normalized to a volume of seven cubic centimeters. (B) Qualitative values. Values were calculated on a

scale of 0-5. 0 corresponding to 0 %, 1 corresponding to 1-20 %, 2 corresponding to 21-40%, 3 corresponding to 41-60%, 4 corresponding to 61-80 % and 5 corresponding to 81-100%.

Table 4. Radiocarbon sample metadata and ages. Dating way by accelerator mass spectrometry and carried out at The University of California Irvine (Keck Carbon Cycle Program) and the Poznan Radiocarbon Laboratory, Poland. We converted ^{14}C dates to calibrated years BP using the Calib 7.0 program (http://calib.qub.ac.uk/calib/calib.html) and the Intcal13 radiocarbon curve (Reimer et al. 2013).

Figure Captions

Fig. 1. Study area on the northern Seward Peninsula, Alaska. Claudi and Jaeger lakes are labeled A and B, respectively. White dots on lakes Claudi and Jaeger indicate sediment coring locations. Image: © SPOT 2008-09-29.

Fig. 2. Geomorphology of northern Seward Peninsula field location (A) Upland yedoma, (B) thermokarst lakes forming in upland yedoma (top image Claudi lake, bottom image Jaeger lake), (C) drained upland yedoma thermokarst lake, (D) Lowland areas affected by drainage of thermokarst lakes and formation of later-generation thermokarst lakes in drained lake basins (images courtesy of L. Plug).

Fig. 3. Schematic of facies distribution in Claudi lake. Y axis shows depth from the lake water surface and X axis shows distance from the margin of Claudi Lake along the coring locations shown in Fig. 1A. Inverted U-shapes and U-shapes indicate the presence of a

baydjerakh top or baydjerakh low at the coring site respectively. The presence of tephra bands and inclusions greater than one centimeter in thickness is indicated by a “T” symbol. Asterisk symbol indicates location of cores sub sampled for biogeochemical ($\delta^{13}C$, C/N, TOC) and macrofossil analysis. Plus symbol indicated location of cores sub sampled for grain size. “O” symbol indicates location of core shown in Fig. 4.

Fig. 4. Schematic of facies distribution in Jaeger Lake. Y axis shows depth from the lake water surface and X axis shows the distance from the margin of Jaeger lake along the coring locations shows in Fig. 1B. Inverted U-shapes indicate the presence of baydjerakh tops at the coring sites. The presence of tephra bands and inclusions greater than one centimeter in thickness is indicated by a “T” symbol. Asterisk symbols indicate location of cores used for biogeochemical analysis ($\delta^{13}C$, C/N, TOC) and macrofossil analysis.

Fig. 5. High resolution images of examples of the four key facies identified. From left to right: F1 massive silt lacking aquatic macrofossils and other aquatic indicators, F2 interbedded organic silt, F3 chaotic silt, and F4 silt-rich mud. Images are from different coring locations in both Claudi and Jaeger lakes. Scale bar is 10 cm in length. Image brightness and contrast were adjusted to enhance sediment features.

Fig. 6. Downcore analysis of sediment cores from lake Claudi center. Macrofossil analysis standardized to 7 cc. Scale bars marked 0-5 are qualitative macrofossil observations. For core location see Fig. 5, where this core is indicated by an “O” symbol.

Fig. 7: Relationship between facies thickness and distance from margin for silt-rich lake mud (solid fill) and basal facies combined (no fill). The x-axis shows distance from margin in meters. The y-axis shows average thickness of facies at that location in centimeters.

Fig. 8. Schematic diagram showing the evolution of facies distribution in yedoma-type thermokarst-lake development. In the initial stage (A) a disturbance (such as climate change, wild fire or construction by people) causes disturbance to the ground thermal regime. In stage (B) flooding of the formerly subaerial surface leads to the formation of F2. In (C), as vertical subsidence and lateral erosion deepen the lake, F1 (talik) forms beneath the lake, freeze-thaw processes deform or rework F2 deposits resulting in the formation of F3, and a central lake basin becomes established where F4 begins to accumulate. In stage (D), lake-bottom baydjarakh topography becomes more pronounced as ice-wedge thaw progresses downward. Reworking by wave action of material from F3 at the lake margin results in continued deposition of F2. F4 continues to accumulate in the center of the lake and also towards the lake margin. During stage (E), excess ice completely disintegrates beneath the lake center, downward thaw bulb growth continues, the lake bottom begins to flatten from the center outwards as the baydjerakh topography infills.

Figure 1

Click here to download high resolution image

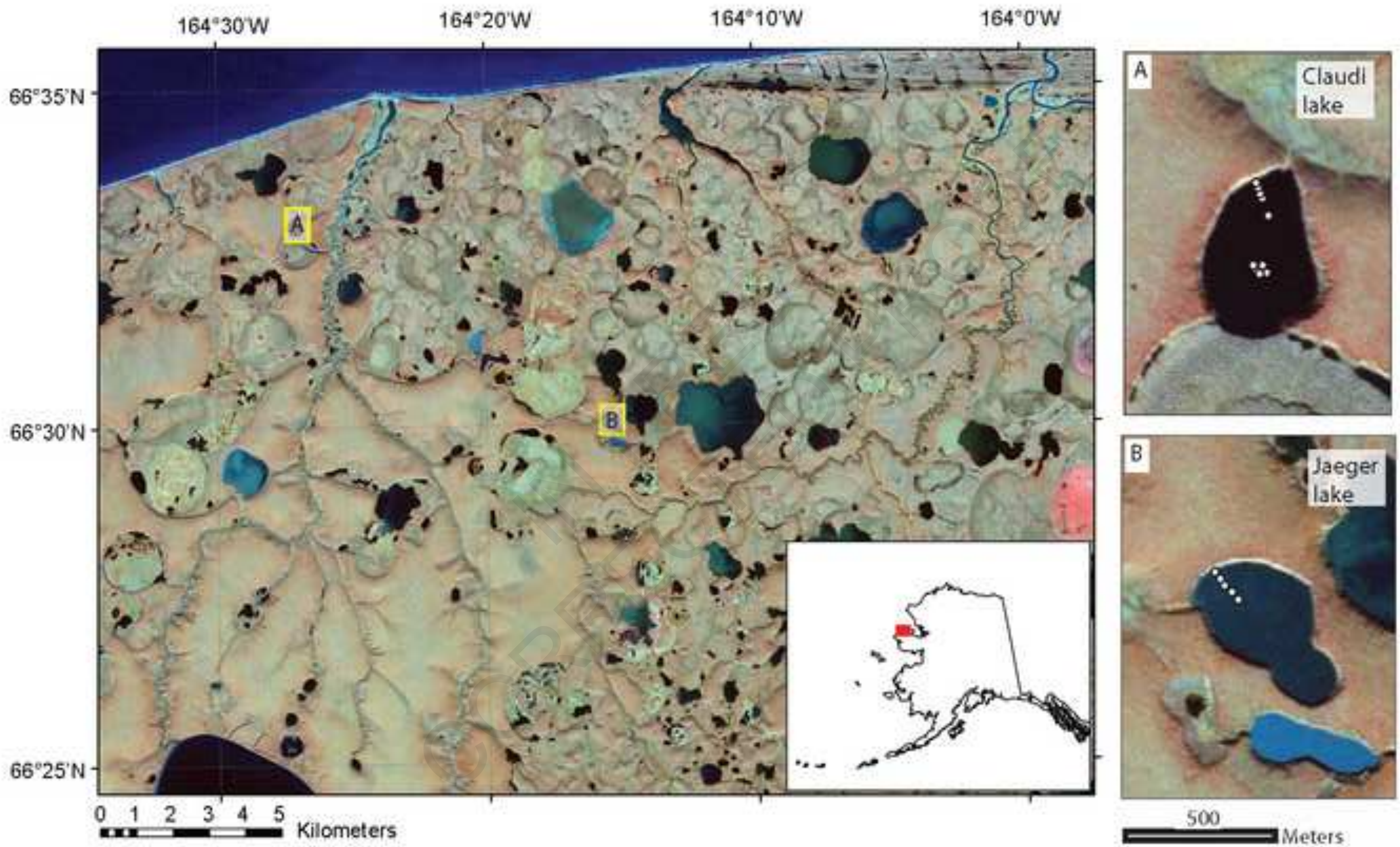

Figure 2

Click here to download high resolution image

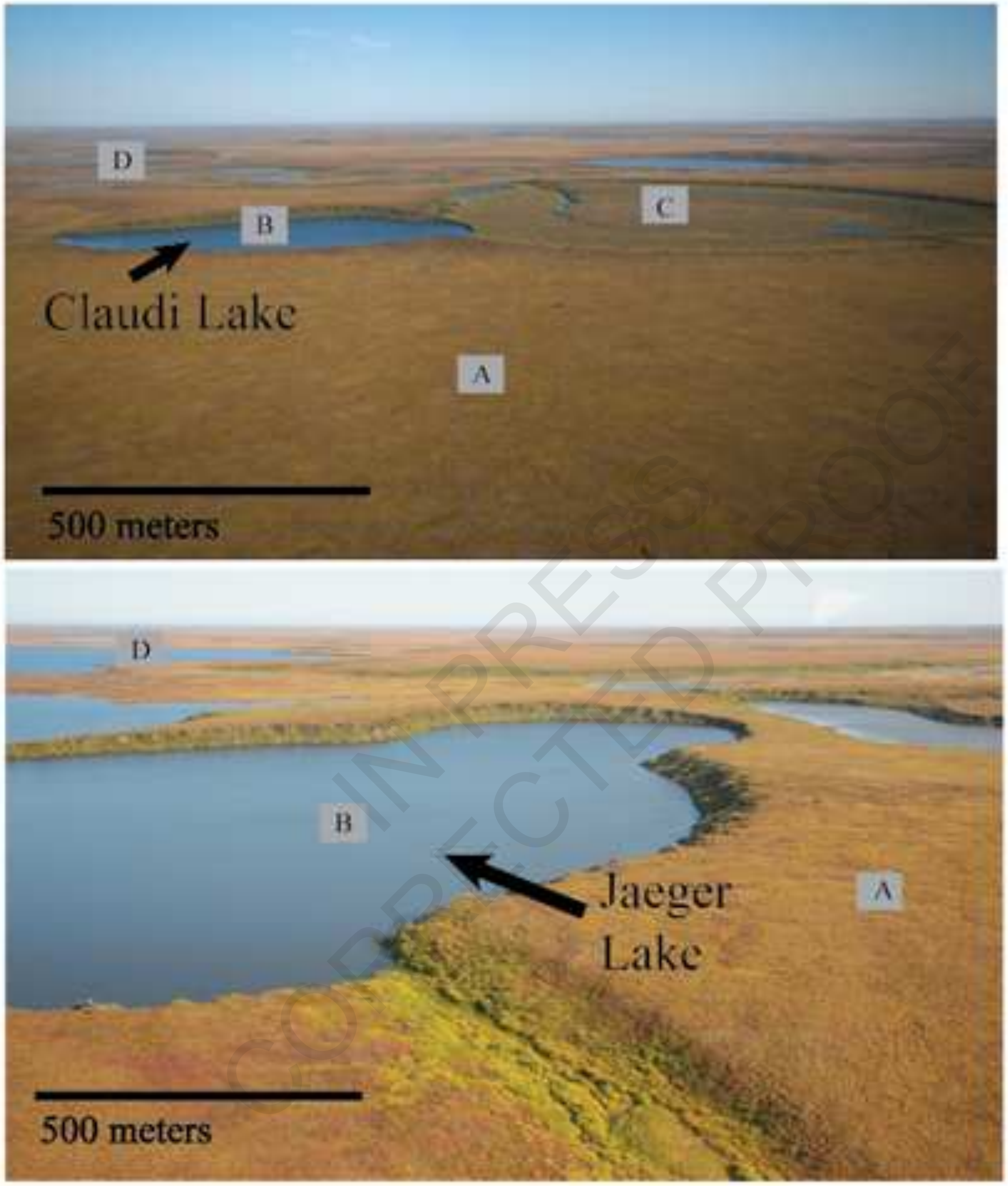

Figure 3

Click here to download high resolution image

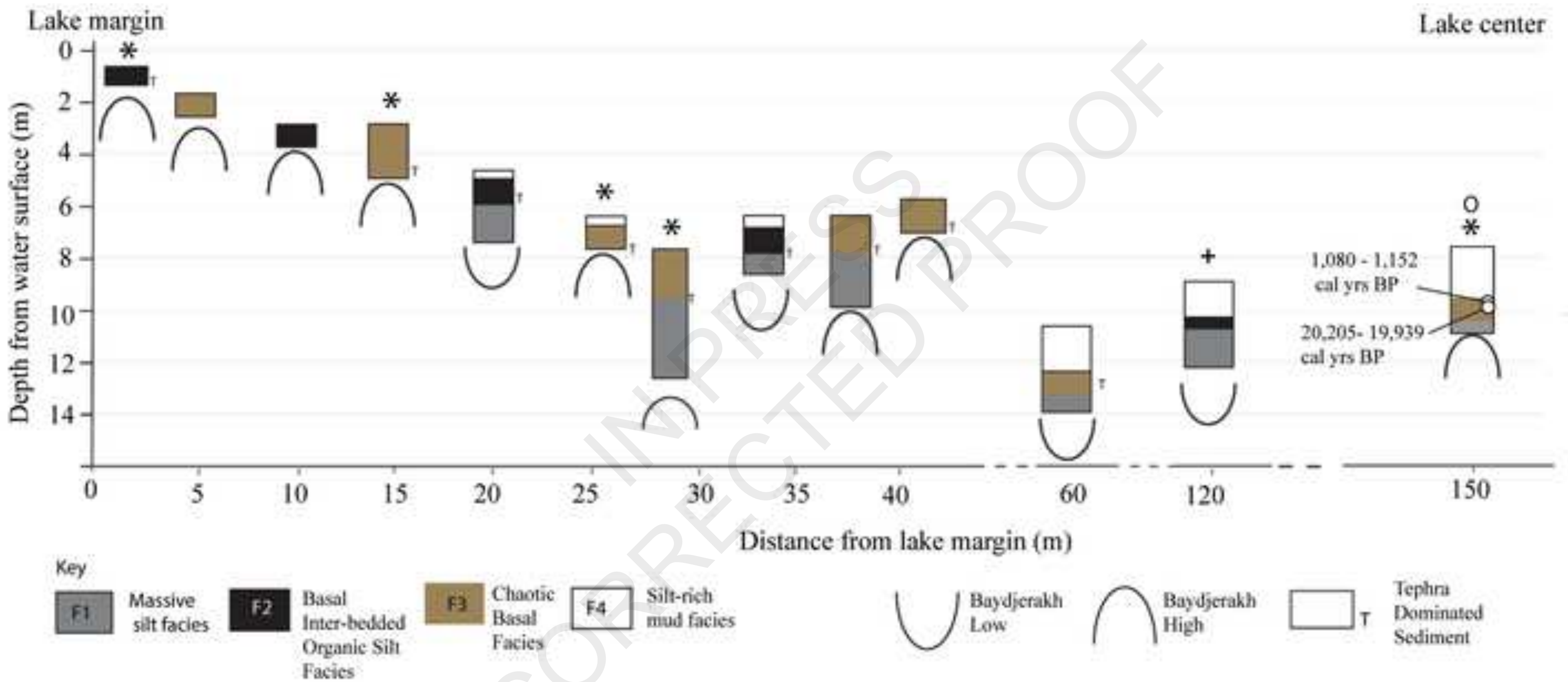

Figure 5

Click here to download high resolution image

Figure 6

Click here to download high resolution image

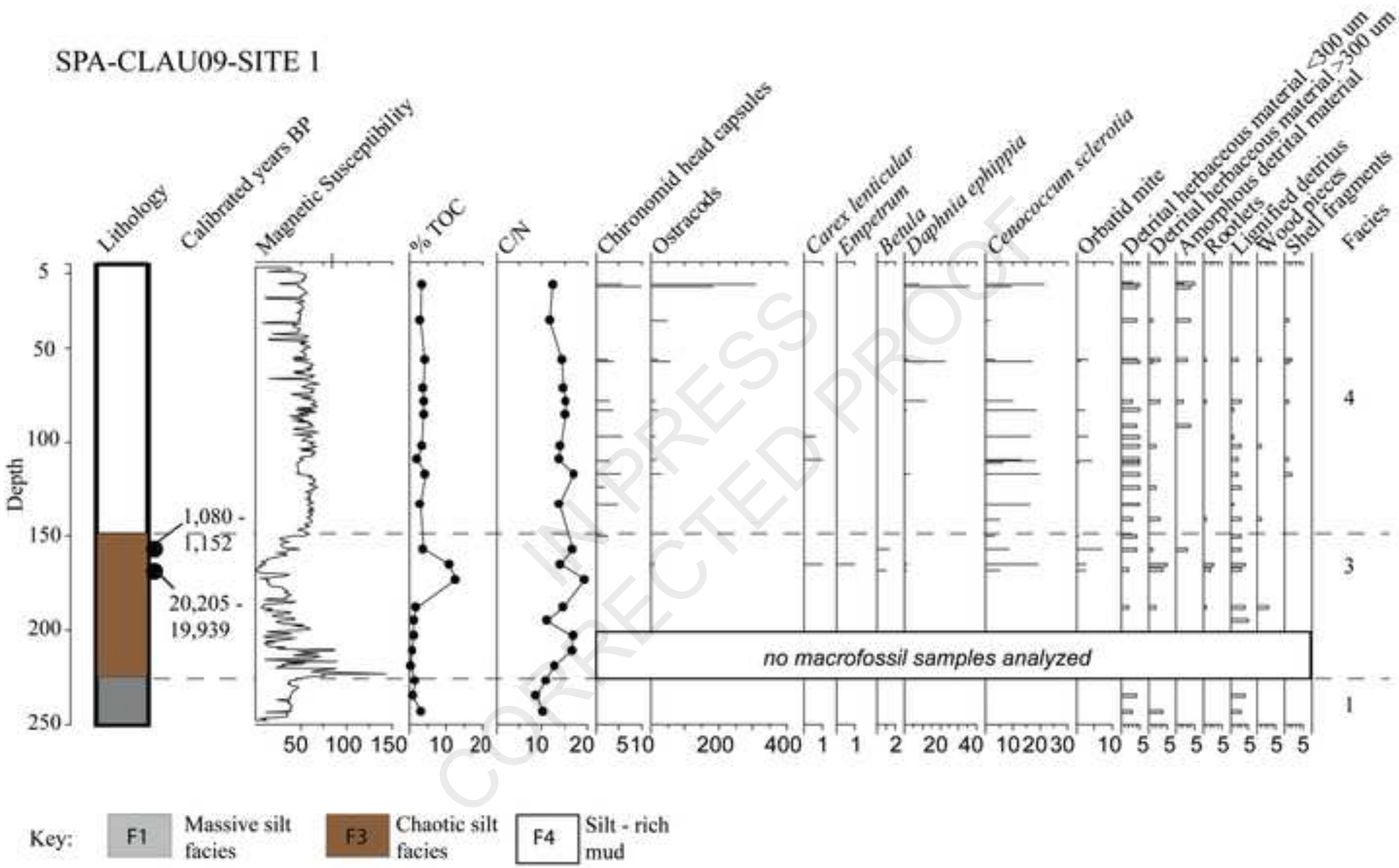

Figure 4

Click here to download high resolution image

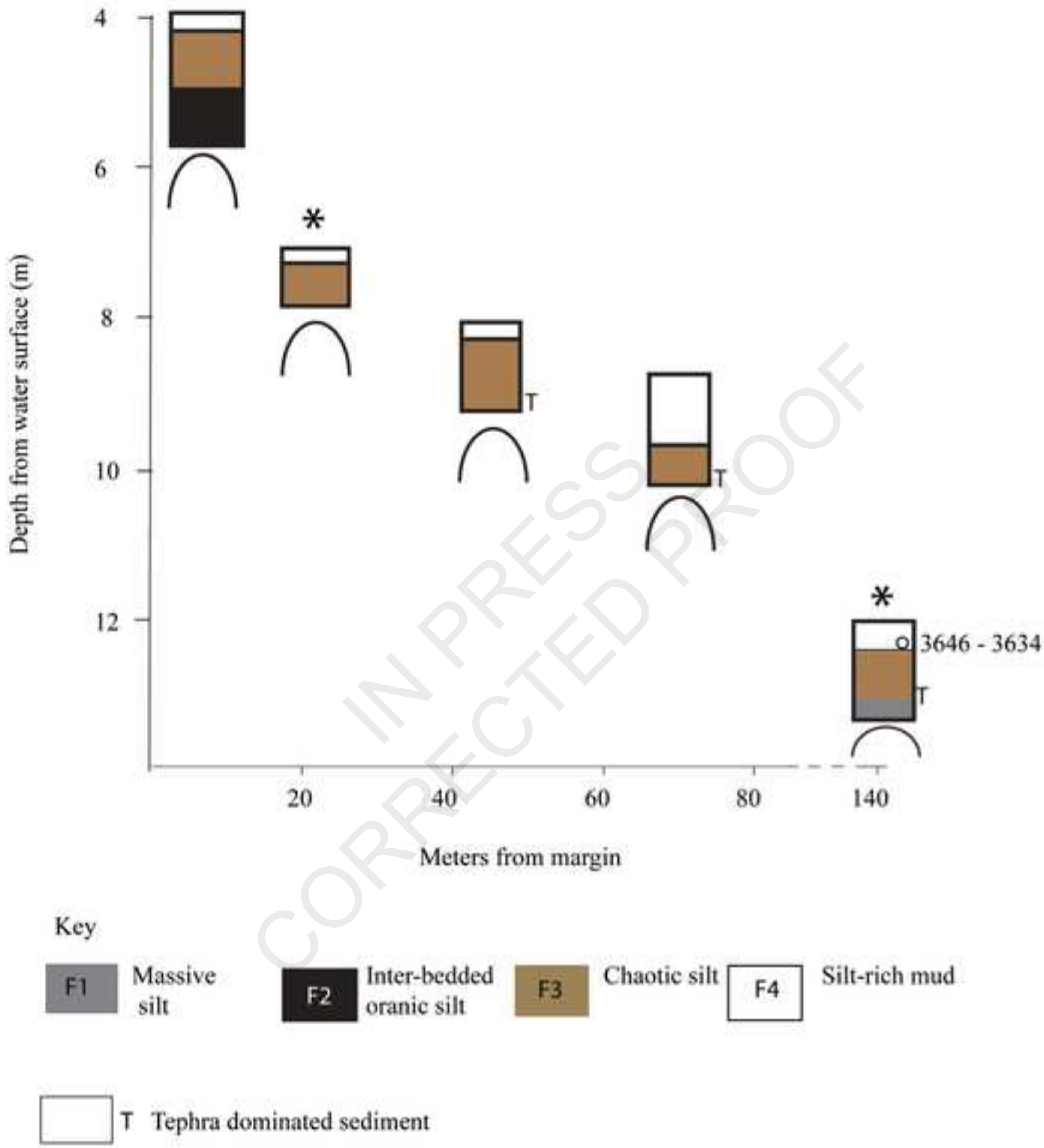

Figure 7
Click here to download high resolution image

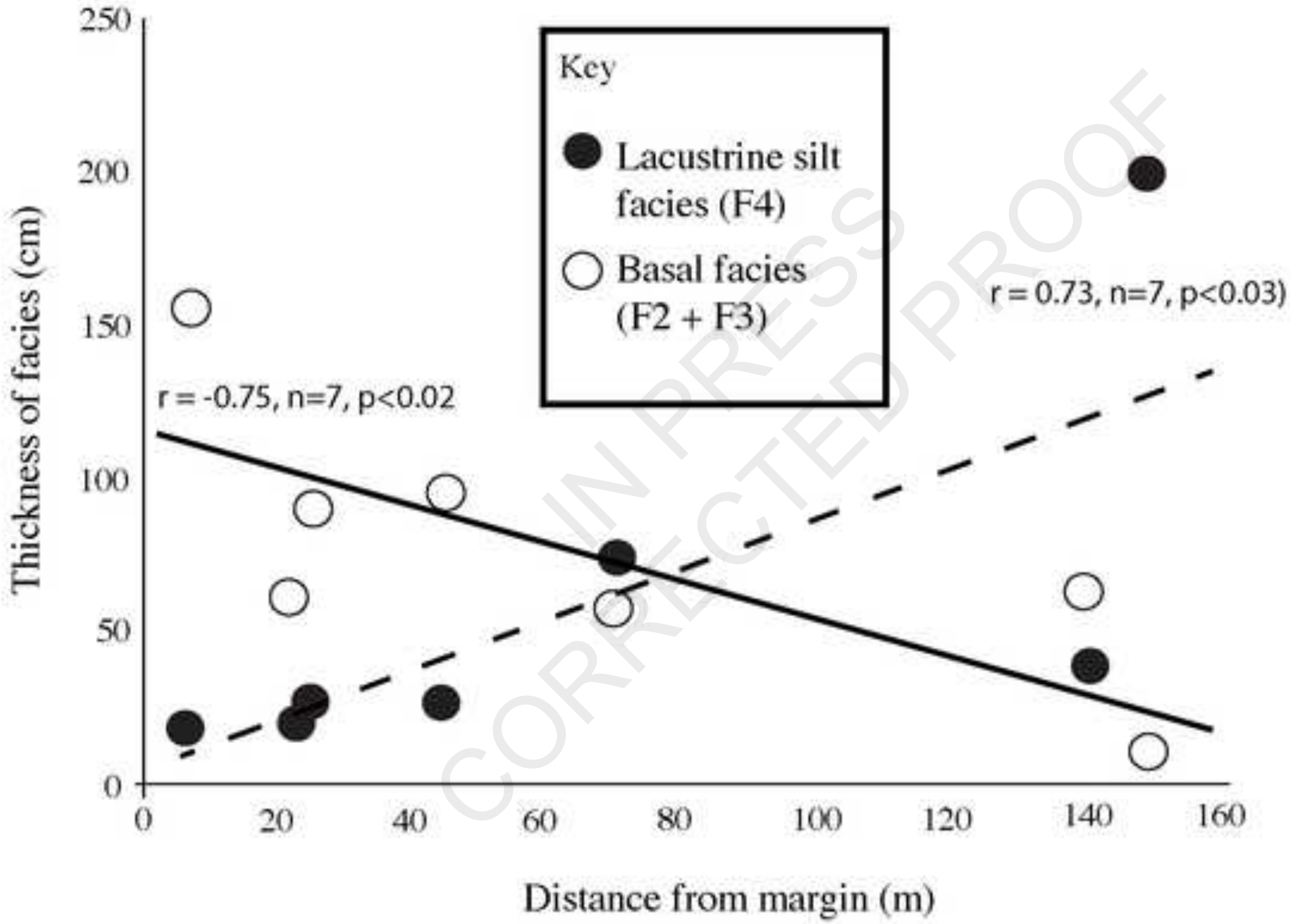

Figure 8
Click here to download high resolution image

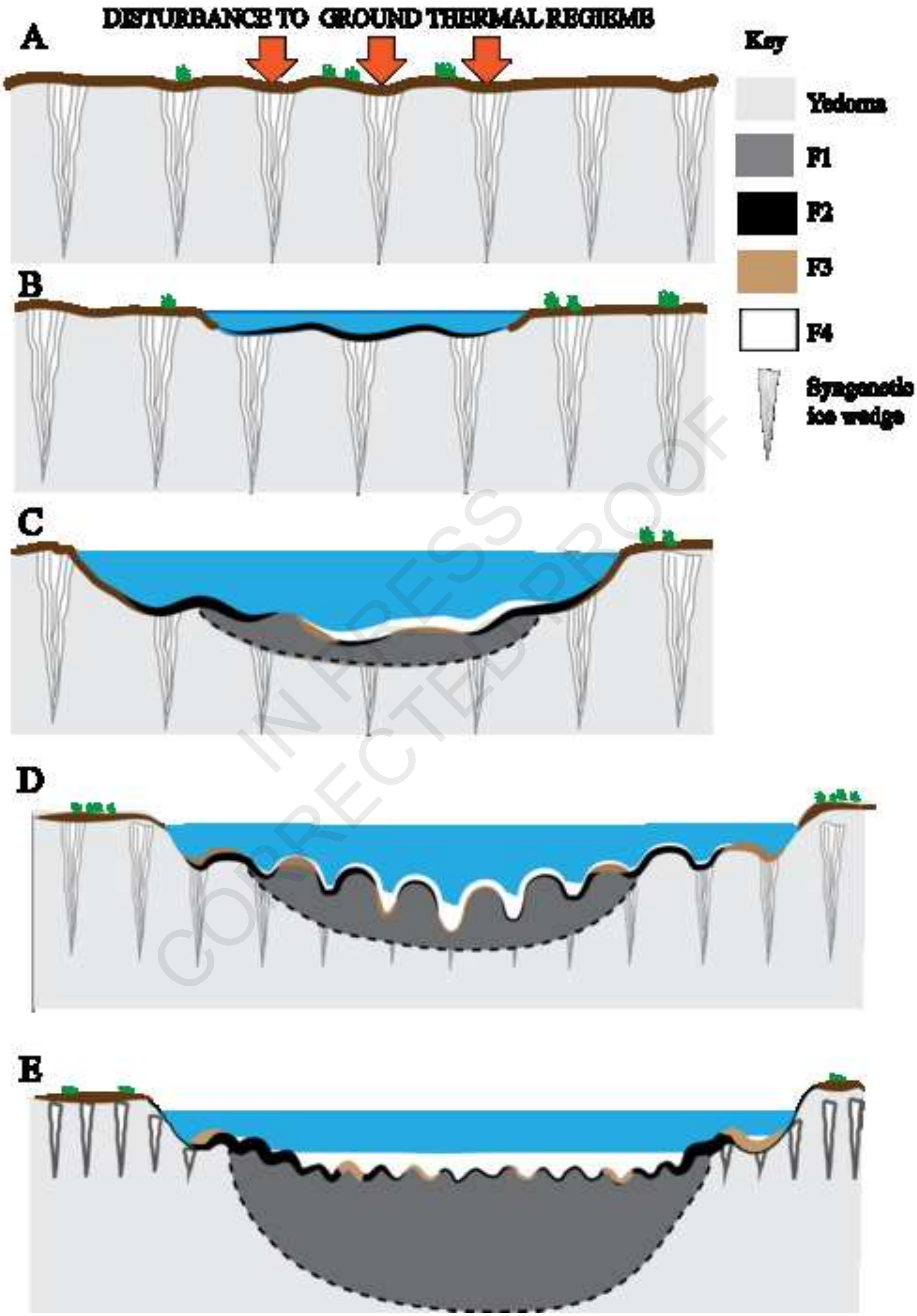

Table 1
Click here to download Table: Table 1.xlsx

Lake name	Lake depth (max, m.)	Secchi disk depth (m)	Long axis (m)	Short axis (m)	Area (ha)	Freeze to bottom	Latitude	Longitude	Elevation (m above sea level)	Parent material	Drainage outlet?
Jaeger	12.73	no data	732	217	24.06	no	66° 30'1.27"N	164° 15'21.35"W	44	upland yedoma	yes, active
Claudi	9.20	3.40	575	397	16.27	no	66° 33'05.80"N	164° 27'01.37"W	24	upland yedoma	yes, inactive

Table 3
Click here to download Table: Table 3.xls

	F1: Massive silt (n=7)	F2:Inter-bedded silt (n=21)	F3: Chaotic silt (n=18)	F4: Silt-rich mud (n=45)
A: Quantitative: mean number of discrete macrofossils per 7 cc				
Chironomid head capsules (aquatic)	0.00	0.43	0.05	3.36
Ostracod half shell (aquatic)	0.00	1.90	0.90	47.02
Daphnia ephippia (aquatic)	0.00	0.25	0.00	2.56
Seeds (terrestrial and aquatic)	0.39	0.79	0.15	0.12
Fungal resting body (terrestrial)	0.00	11.18	0.00	4.51
Oribated mite (terrestrial)	0.00	4.68	0.16	0.45
Bract (terrestrial)	0.00	0.25	0.00	0.00
B: Qualitative: mean assigned qualitative value (0-5)				
Detrital herbaceous material: fine <300 um	3.00	3.67	4.39	2.20
Detrital herbaceous material: coarse >300 um	1.00	3.00	1.11	0.80
Amorphous detrital material	0.00	0.25	1.16	0.00
Rootlets	0.00	1.38	0.22	0.30
Lignified detritus	2.86	2.91	1.09	2.70
Wood fragments	0.86	0.60	0.09	1.00
Moss leaflets	0.00	0.31	0.69	0.10
Insect fragments	0.14	0.46	0.16	0.40
Shell fragments	0.00	0.10	0.74	0.00

Table 4

Click here to download Table: Table 4.xls

Lab ID	Core ID	Material dated	Facies	Depth below sediment water	Radiocarbon years BP	^{14}C age calibrated intercept	Comment
UCIAMS21194	Jae09-5A-1N-1	terrestrial herbaceous	F4	72 - 74	4825 +/- 20	3646-3634	Minimum lake age
POZ-63619	Clau09-1D-1U-1	terrestrial leaf fragment	F3	166- 168	940 ± 35	1080-1152	Minimum lake age
UCIAMS21196	Clau09-1D-1U-2	terrestrial herbaceous	F3	234 - 236	18170 +/- 80	20205-19939	Reworked material
UCIAMS21210	N/A	modern *Drepanocladus* spp.	N/A	N/A	2495 +/- 20	2658-2568	Age offset due to old carbon effect
UCIAMS21209	N/A	modern *Potamogeton* spp.	N/A	N/A	2260 +/- 20	2403-1658	Age offset due to old carbon

Table 2
Click here to download Table: Table 2.xlsx

Facies	% TOC	C/N	$\delta^{13}C$	grain size (µm)	MS SI	Visual characteristics
Taberal Silt (F1)	(n=13)	(n=13)	(n=13)	(n=10)	(n=187)	massive grey (5 Y 4/1) silt matrix containing occasional peat and tephra balls, lenses or distorted
Median	2.00	10.93	-25.55	26.4*	24.30	
Range	0.6 to 5.1	8.67 to 13.46	-28.35 to -21.02	18.54 to 29.3	9.3 to 157.6	
Inter-bedded Basal (F2)	n=24	n=24	n=24	no data	n=287	alternate bedding of silt, organic detrital material and tephra varying in width from 1-10 cm, with diffuse boundaries
Median	2.77	13.43	-26.09	no data	43.50	
Range	0.12 to 31.83	5.68 to 21.26	-27.80 to -24.28	no data	0.2 to 199.5	
Chaotic Basal (F3)	n=14	n=14	n=14	n=3	n=399	a silt matrix of either brown or grey (5Y 3/1, 5 Y 4/3), showing signs of disturbance, with tephra and peat inclusions
Median	1.61	12.50	-25.70	28.6*	26.00	
Range	0.30 to 12.32	8.81 to 16.89	-28.13 to -23.62	23.92 to 28.70	2 to 169.9	
Lacustrine Silt (F4)	n=46	n=46	n=46	n=29	n=915	fine brown silt (2.5Y 3/1, 2.5Y 3/2, 5Y 3/1 or 5Y 3/2), often displaying darker laminations (and10YR 2/1 to 10YR 3/2)
Median	3.93	13.42	-27.03	22.10*	47.20	
Range	1.08 to 13.09	9.74 to 22.69	-28.56 to -23.77	19.38 to 28.32	0.3 to 132.4	

Supplementary material A
Click here to download Supplementary material for on-line publication only: Supplimentary material A.xlsx

Supplementary material B

Click here to download Supplementary material for on-line publication only: Supplimentary material B.xlsx

Supplementary material C

Click here to download Supplementary material for on-line publication only: Supplimentary material C.xlsx

Interactive Map of study lakes

Click here to download Interactive Map file (.kml or .kmz): Study lakes.kmz